A maze of solid solutions of pimobendan enantiomers: an extraordinary case of polymorph and solvate diversity

Toms Rekis,*,†,‡ Agris Bērziņš,† Inese Sarceviča,† Artis Kons,† Mārtiņš Balodis,†,¶ Liāna Orola,† Heike Lorenz,‡ and Andris Actiņš†

†*Department of Physical Chemistry, University of Latvia, Riga, Latvia*

‡*Max Planck Institute for Dynamics of Complex Technical Systems, Magdeburg, Germany*

¶*Ecole polytechnique fédérale de Lausanne, Lausanne, Switzerland*

E-mail: toms.rekis@lu.lv

Abstract

Over ten polymorphs and solvatomorphs of chiral pharmaceutically active ingredient pimobendan were found to lack enantioselectivity in the solid state, accordingly, forming solid solutions of enantiomers, which is reported to be a rare phenomenon. Solid form screening was performed on different enantiomeric composition samples to analyse obtained phases with PXRD and TG/DSC. For non-solvated forms a melt phase diagram has been constructed convincingly showing existence of stable and metastable solid solutions near the pure enantiomer and around the racemic composition regions. A crystal structure study combined with solid-state NMR experiments was performed to analyse and explain structural aspects of pimobendan solid solutions. Furthermore, driving force for existence of such a surprisingly large amount of different solid state phases lacking enantioselectivity for a single compound is elucidated tracking down the origin of their formation to the molecular level.

Introduction

Chirality plays a significant role in many divisions of science. Particularly important it is in pharmacy, agrochemistry, and food industry where occasionally a single molecule with a specific configuration is desired over a mixture of enantiomers or diastereomers.[1] Therefore increasing number of studies have been conducted to investigate the routes for obtaining a single enantiomer.[2] Besides the enantioselective synthesis a set of physicochemical methods are extensively used for the separation of enantiomers which involve solid crystalline phases of the compound of interest.[2,3] Understanding the enantioselectivity in the solid state is therefore crucial.

Usually chiral substances show very high enantioselectivity at the crystallization stage. More than 99 % of racemic enantiomeric mixtures are reported to crystallize either forming racemic compounds or conglomerates,[3] where former is a racemic crystalline phase with a strict order of both components, and latter contains two crystalline (mirror) phases where each component has formed its own phase. Extremely rarely, however, single phases form where there is only partial or no recognition of the enantiomers in the solid state.[3–7] Consequently scalemic compositions are able to form isostructural phases. Such solid solutions are an interesting phenomenon since it hides the answers on how the enantioselectivity is governed in the solid state.

From a structural point of view two cases can be distinguished regarding enantioselectivity in the solid state: 1) complete lack of enantioselectivity (Type I); 2) partial enantioselectivity is present (Type II). Type I has been defined as follows: within a crystal containing x R molecules and $(1-x)$ S molecules the probability of finding an R molecule on a given site is proportional to x, and the probability of finding an S molecule is proportional to $(1-x)$.[8] Two compounds have been reported to belong to this case by the authors of the classification.[8,9] Furthermore, two mandelic acid derivatives[10,11] can be classified as Type I solid solutions as there is only one symmetrically independent site in the unit cells of the respective enantiopure structures. Consequently, no partial enantioselectivity is possible as for that at least two

symmetrically independent sites are required in the enantiopure structures.[8] Type II in the present study is left for structures showing certain degree of enantioselectivity which arises from reasonable structural aspects. The definition of Type II has been therefore slightly revised compared to that introduced decades ago in the pioneering study of structural aspects of solid solutions of enantiomers.[8] As it can be observed in several structures determined recently[6,12] for which partial enantioselectivity is evidently present the structural aspects do not fully correspond to the given definition, which rather describes an idealized case of partially enantioselective solid solutions. For Type II solid solutions ($Z' \geq 2$) the asymmetric molecules in the enantiopure structures are typically *quasi*–centrosymmetrically related, which is achieved by different conformations of the molecules of the same handedness. In such cases a single enantiomer is forming a *quasi*–centrosymmetric structure. When the opposite enantiomer is introduced genuine centrosymmetry can be achieved locally. At the racemic composition a true racemic compound (an ordered centrosymmetric structure) is possible, however, usually some degree of disorder is observed. Nevertheless, the racemic structure can be solved in a centrosymmetric supergroup of the Sohncke space group of the enantiopure structure. Consequently, the value of Z' is halved. These structural aspects are well illustrated with a phenylpiracetam solid solution example[6] where two pairs of *quasi*–centrosymmetric molecules are present in the enantiopure structure (see Figure 1). There is a pseudoinversion centre (depicted with a closed circle) in the enantiopure structure

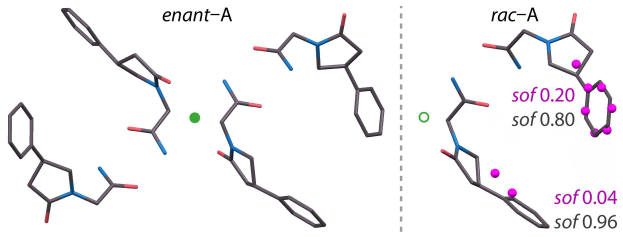

Figure 1: Asymmetric units of phenylpiracetam solid solution α limiting cases *enant*–A ($P1$, $Z' = 4$) and *rac*–A ($P\bar{1}$, $Z' = 2$)[6] showing disorder with corresponding site occupancy factor (*sof*) values give.

and a statistical inversion centre in the racemic structure. For both asymmetric sites in the

racemic structure there is a probability of finding R or S enantiomer of phenylpiracetam. This probability, however, is not 50 %. One of the sites is nearly ordered showing disorder as low as 4 %, the other one is largely ordered. From the structure of racemic phenylpiracetam alone it is evident that at a certain degree the enantiomers are recognized in the solid state. Several other compounds possessing exactly the same structural features and consequently having partial enantioselectivity are reported (tazofelone,[13] citalopram oxalate,[14] atenolol,[15] carvedilol phosphate,[16] timolol maleate,[17] and two naphthalimide derivatives[12]). Such structures correspond to Type II solid solutions.

In this study a chiral pharmaceutically active ingredient pimobendan (4,5-Dihydro-6-[2-(*p*-metoxyphenyl)-5-benzimidazolyl]-5-metyl-3(2H)-pyridazinone) has been investigated. Pimobendan is used to treat heart failure either in veterinary or human medicine.[18,19] The chemical scheme of pimobendan is shown in Figure 2. In this study pimobendan is found

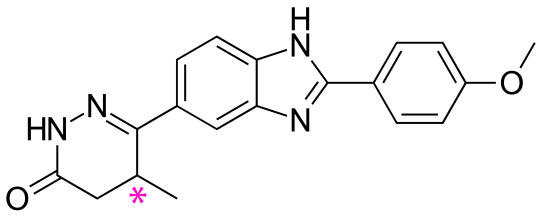

Figure 2: Chemical scheme of pimobendan (4,5-Dihydro-6-[2-(*p*-metoxyphenyl)-5-benzimidazolyl]-5-metyl-3(2H)-pyridazinone).

to form a variety of polymorphs and solvates in its racemic and enantiopure form. Furthermore, it is an extraordinary case as more than ten of the non-solvated and solvated forms are proven to be solid solutions, while also the others are in fact not strictly classified as enantioselective.

The aim of this study was to present the known solid form diversity of racemic and enantiopure pimobendan, characterize the solid solutions of the compound, and finally to track down the structural aspects responsible for the formation of such a large number of non-enantioselective crystalline phases.

Experimental Methods

Materials

Racemic pimobendan (>99.8 %) was supplied by JSC *Grindeks* (Riga, Latvia). Pure enantiomer of pimobendan was resolved from the racemic mixture by classical resolution using (–)–*O*,*O*'–dibenzoyl–L–tartric acid according to method available in patent literature.[20] The method was not further optimized as a result the yield for the enantioseperation was as low as around 4 %, similarly as given in the source. Purity (99.7 % *ee*) was confirmed by chiral chromatography. (–)–*O*,*O*'–dibenzoyl–L–tartric acid, phosphorus pentoxide, aqueous ammonia were purchased from commercial sources. Solvents used in the study were HPLC grade or intended for organic synthesis with purity >99 %. Water (<0.01 µS cm^{-1}) was deionized at the laboratory using ion-exchange resins.

Polymorph and solvate screening

Solid form screening was performed on racemic pimobendan by crystallizing from different solvents, desolvating solvates, exposing solid forms to solvent vapours, and annealing the amorphous form at elevated temperatures. Stoichiometry of solvates was elucidated based on repeated TG studies. Detailed procedures for obtaining presented pimobendan crystal forms are given in the Supporting Information.

Extensive solid form screening of enantiopure pimobendan, however, was not performed, since it is not available on the market, and classical resolution of pimobendan enantiomers gave extremely low yields. However, a few forms have been obtained via crystallization from different solvents.

Single crystals

Single crystals of pimobendan form *rac*–A were grown by slow evaporation of a dry acetonitrile and ethyl acetate solution (1:1 v/v) at room temperature in a P_2O_5 dessicator (to

prevent the formation of the monohydrate due to air moisture) over the course of several months.

SCXRD

The data were collected at 293 K temperature on a Bruker Nonius Kappa CCD diffractometer using Mo-Kα radiation (graphite monochromator, wavelength of 0.710 73 Å) (*Bruker*, Germany). The structure was solved by direct methods and refined by full-matrix least squares on F^2 for all data, using SHELX-2014 software suite.[21] The non-hydrogen atoms were refined anisotropically. As disorder was found, the site occupancy factors (*sof*) of atoms were refined using SHELX command PART and an additional free variable.

PXRD

PXRD patterns were determined on a Bruker D8 Advance diffractometer (*Bruker*, Germany) using copper radiation (Cu-Kα) at a wavelength of 1.541 80 Å equipped with a LynxEye position sensitive detector (*Bruker*, Germany). The tube voltage and current were set to 40 kV and 40 mA. The divergence slit was set at 0.6 mm and the antiscattering slit was set at 8.0 mm. The diffraction pattern was recorded using a scanning speed of 0.2 s/0.02° from 3° to 35° on 2θ scale.

For indexation or structure determination PXRD patterns were recorded on a Bruker D8 Discover diffractometer (*Bruker*, Germany) using copper radiation (Cu-Kα) at a wavelength of 1.541 80 Å equipped with a LynxEye (1D) detector in transmission mode. The tube voltage and current were set to 40 kV and 40 mA. The samples were loaded into special glass Nr. 10 capillaries (0.5 mm in diameter). Capillary spinner (60 rpm) was used to minimize instrumental and sample packing aberrations. Upper knife edge was used to reduce the background produced by air scattering and lower knife edge was used to block the primary beam. The diffractometer incident beam path was equipped with a Göbel mirror, Soller slit, and a 0.6 mm divergence slit, while the diffracted beam path was equipped only with Soller

slit. The diffraction patterns were recorded on 2θ scale from 3° to 70° with 0.01° increments, using a scan speed of 36 s per step.

Structure determination from PXRD data

Indexing, space group determination, structure solution, and Rietveld refinement were performed using EXPO2014.[22] The unit cell dimensions were determined by applying the N-TREOR09[23] and Dicvol06[24] indexing procedures, with a set of 20–25 reflections found in 3° to 30° 2θ range. Space group determination was carried out using a statistical assessment of systematic absences, and Z' was determined based on solid-state NMR (SSNMR) results. The cell and diffraction pattern profile parameters were refined according to the LeBail algorithm.[25] The background was modelled by a 20th order polynomial function of the Chebyshev type, peak profiles were described by the Pearson VII function.

The initial geometry of molecules was taken from the crystal structure of *rac*–A. The Monte Carlo/Simulating Annealing technique was used to constantly adjust the conformation, position, and orientation of the trial model in the unit cell in order to maximize the agreement between calculated and measured diffraction data. The Rietveld refinement was carried out using soft constraints on bond distances and angles. In the Rietveld refinement, profile and cell parameters, isotropic thermal vibration, and preferred orientation parameters (using March-Dollase model[26,27]) were optimized to get the optimal crystal structure. The planar conjugated rings were separately treated as rigid bodies, whereas soft constraints on bond distances and angles were used. The final Rietveld refinement showed a good agreement between the observed and the calculated profiles.

After the Rietveld refinement the atomic positions of the final structure were relaxed in Quantum ESPRESSO[28] using the PBE functional with ultra-soft pseudopotentials from the original pseudopotential library and a 44 Ry planewave cut-off energy with vdW interactions treated according to the D2 method of Grimme.[29] The parameters of convergence, pseudopotentials and the k-point grid were used as suggested for structure optimizations of organic

molecules.[30] The relaxed structure was compared to the refined one to check for the reliability of the structure solution. Atomic positions did not differ significantly. The experimental and calculated PXRD patterns including difference function and Bragg positions are given in Figure S14. Furthermore, SSNMR spectrum of the refined structure was simulated (see below) and compared to that of the experimental one obtaining a good correlation between the experimental and calculated chemical shifts.

Thermal methods of analysis

The TG/DSC curves were obtained using a TG/DSC STAR^e System (*Mettler Toledo*, Switzerland). A 5 to 10 mg sample was weighed on an open aluminium pan and heated at the rate of 5 to 10 $\mathrm{K\,min^{-1}}$ from 25 °C to 250 °C under a continuous nitrogen flow (100 $\mathrm{mL\,min^{-1}}$). The DSC curves were recorded on a SETARAM DSC 131 instrument (*SETARAM Instrumentation*, France) at the heating rate of 0.5 to 5 $\mathrm{K\,min^{-1}}$. Temperature and enthalpy calibration was done using indium, tin and lead reference materials. A 4 to 10 mg sample was weighed in an aluminium crucible and the crucible was crimped.

Melt phase diagram

The mixtures of different compositions were prepared by weighing racemic and enantiopure samples on analytical balance ($d = 0.1$ mg). Different enantiomeric composition samples were then fully dissolved in acetonitrile/ethyl acetate (1:1 v/v) and crystallized in dry conditions. After complete evaporation of the solvent the samples were homogenized in a mortar prior the DSC measurements. For the metastable solid solutions δ and γ the respective forms were obtained by desolvating the hydrate H1 and methanol solvate MS2, respectively. The samples then were homogenized in a mortar prior the DSC measurements. PXRD analysis were performed to analyse obtained products. The DSC analyses were performed as described above. For construction of the solidus lines the onset temperatures of the respective DSC peaks were taken. The DSC peak maxima were used for determination of the corresponding

liquidus lines.

^{13}C SSNMR spectroscopy

Spectra of pimobendan *rac*–D and *enant*–F were recorded at a nominal temperature of 300 K with a Bruker Avance-III 11.7 T spectrometer equipped with a 3.2 mm low-temperature CP-MAS probe operating at Larmor frequencies of 500 and 125 MHz for ^{1}H and ^{13}C, respectively. ^{13}C CP-MAS NMR spectra were recorded at 12.0 kHz. ^{13}C chemical shifts were referenced to the CH_2 resonance observed for adamantane at 38.48 ppm with respect to the signal for neat TMS.[31]

Simulation of solid-state NMR spectra

Chemical shift calculations for *enant*–F and *rac*–D were carried out using the GIPAW method implemented in CASTEP 6.0 software,[32–35] after geometry optimization by relaxing all atomic positions. The calculations were performed with the PBE[36] functional using on-the-fly generated ultrasoft pseudopotentials and a cut-off energy of 600 eV. The Tkatchenko-Scheffler dispersion correction scheme[37] was used. The computed ^{13}C chemical shifts were referenced by linear regression of the computed shielding values to the experimentally observed chemical shifts.[35,38]

Results and Discussion

Polymorphs and solvates of pimobendan

Several crystal forms of racemic pimobendan are already reported in the literature, including pimobendan monohydrate[39,40] (referred to as *rac*–H1 in the present study), pimobendan 1,4-dioxane monosolvate[39] (*rac*–DS1), pimobendan methanol monosolvate[39] (*rac*–MS1), as well as polymorphs *rac*–A,[39,41] *rac*–B,[39,42] and *rac*–D.[40] A recent own study showed existence of

an enantiopure monohydrate *enant*–H5 and its dehydration product — a poorly crystalline form *enant*–E.[40] In the present study, however, several novel crystal forms from racemic pimobendan were obtained, namely, a monohydrate (*rac*–H2), a hemihydrate (*rac*–H3), a trihydrate (*rac*–H4), a methanol hemisolvate (*rac*–MS2), an isostructural non-stoichiometric solvate family (*rac*–G; toluene, cyclohexane, 1,4-dioxane, ethyl acetate, acetone, cyclohexanol, xylene, buthyl acetate, ethyl formate, methyl acetate, propyl acetate, and propyl formate solvates), two polymorphs — *rac*–C, and *rac*–G_d (the isostructural desolvate of solvates *rac*–G). For enantiopure pimobendan along with the already reported hydrate *enant*–H5[40] and its dehydration product (*enant*–E), a 1,4-dioxane monosolvate (*enant*–DS2) and a polymorph (*enant*–F) was obtained. PXRD patterns of all known pimobendan crystal forms are given in Figure 3. The transition scheme between the crystalline forms of racemic pi-

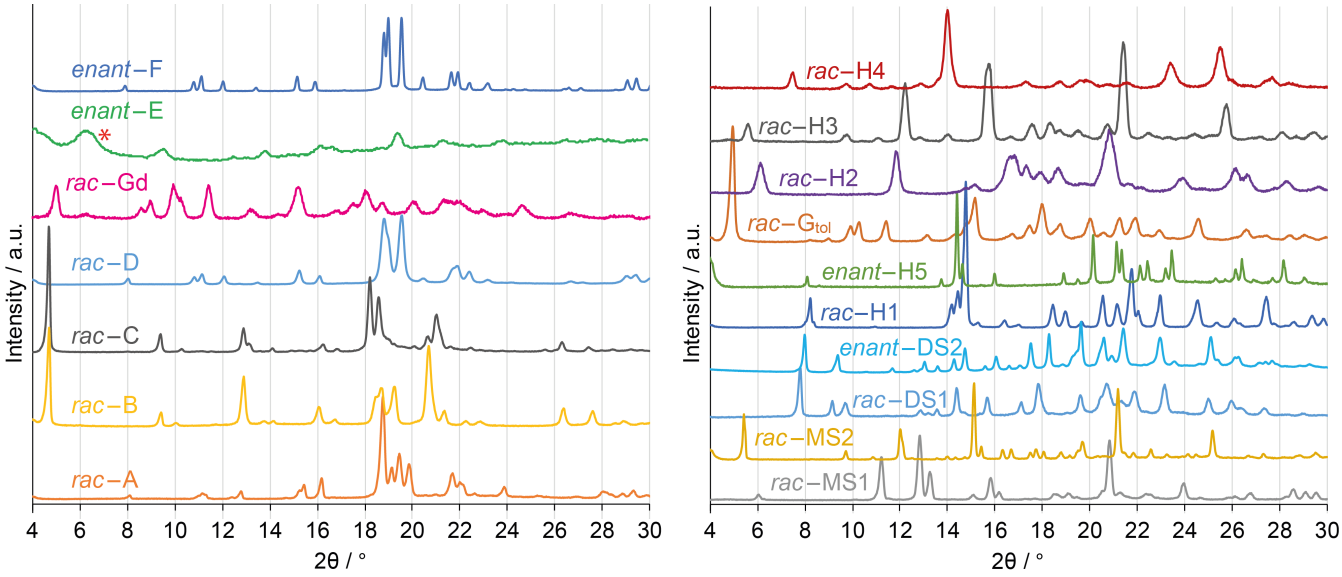

Figure 3: PXRD patterns of non-solvated (left) and solvated (right) pimobendan crystal forms (* – the broad peak observed at 6.3 2θ for *enant*–E arises from the film of the variable temperature chamber).

mobendan is shown in Figure 4 (see also Figure S1 in Supporting Information for transition conditions). In table Table 1 thermochemical data of racemic and enantiopure pimobendan polymorphs is given. From heat of fusion rule[43] it follows that polymorphic form systems *rac*–A and *rac*–D, *rac*–A and *rac*–B, *rac*–D and *rac*–B, and *rac*–D and *rac*–C are monotropic,

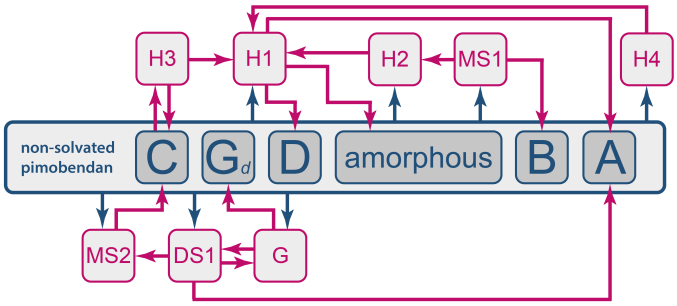

Figure 4: Principal transitions between the crystalline forms of racemic pimobendan (with H, MS, DS, and G solvates with water, methanol, 1,4-dioxane, toluene (or others), respectively).

so *rac*–A is the most stable polymorph in all temperatures while *rac*–D is the second most stable. No relationship between *rac*–B and *rac*–C can be assessed as the enthalpy of melting cannot be determined clearly for the respective forms. Neither any slurry experiments are suitable in this case as both *rac*–B and *rac*–C are not stable in solvents and can be in fact obtained only by desolvating respective solvates of pimobendan and never crystallizing from solvents.

Table 1: Melting onsets and enthalpies of melting of pimobendan crystal forms (* — peak maximum; ** — due to immediate recrystallization event no precise enthalpy of melting can be assessed).

Form	Melting point / °C	ΔH^{f} / kJ mol^{-1}
rac–A	240	40.1
rac–D	224	31.0
rac–B	189*	≈ 25 **
rac–C	176*	≈ 25 **
rac–G_d	163*	≈ 3
enant–F	231	33.2

Extensive system of solid solutions of pimobendan enantiomers

Thermodynamic evidence of solid solution existence of a given two component system can be summarized in a form of a melt phase diagram. Furthermore, it gives a complete picture of the system of interest showing thermodynamic stability and miscibility limits of the existing solid solutions.[6,10,44] The melt phase diagram of pimobendan enantiomers (Figure 5)

shows existence of four different solid solutions, namely, α, γ, δ, and ζ ($\alpha_{X=50}$ corresponds to previously mentioned form *rac*–A, $\gamma_{X=50}$ — to form *rac*–C, $\delta_{X=50}$ — to *rac*–D, and $\zeta_{X=0}$ — to *enant*–F). The DSC and PXRD data used to establish the phase diagram is given in Figures S2–S7. Concerning the thermodynamically stable phases the diagram indicates that there is a eutectic system of two solid solutions (α and ζ), consequently, miscibility is present around the racemic composition and near the pure enantiomer region, similarly like observed, e.g., in the cases of phenylpiracetam[6] and malic acid.[5] Due to experimental lim-

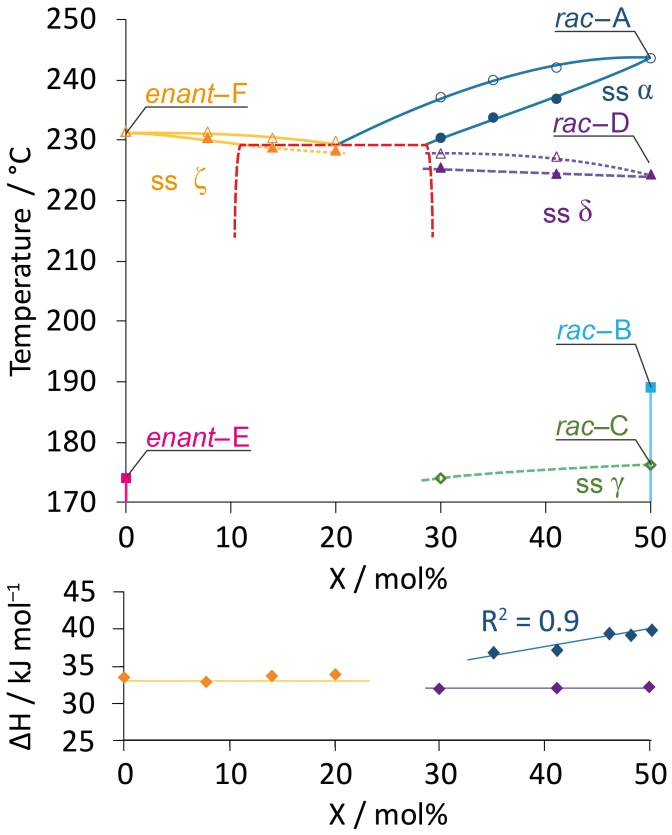

Figure 5: Melt phase diagram of pimobendan enantiomers and Melting enthalpy–temperature plot (in the phase diagram: closed markers — solidus, open markers — liquidus; lines are guides for the eyes).

itations no equilibrated samples could be obtained representing the miscibility gap of solid solutions α and ζ, therefore no eutectics could be experimentally accessed. However, the liquidus lines indicate that the eutectic composition is around 20 %. Therefore, the eutectic temperature is estimated to be of around 229 °C and the miscibility gap existing between

roughly 10 to 30 % composition. There is a good correlation between the enthalpy value and the composition (Figure 5) for α ($R^2 = 0.9$), however, in case of ζ the low coefficient value rather indicate for no significant composition dependent variation of the enthalpy of melting for solid solutions ζ. As shown in the phase diagram, the $\zeta + liquid$ region is relatively flat. It indicates that pimobendan enantiomers tend to form what is called an ideal solid solution. Close-to-ideal behaviour is rare, it is reported for two glycerol ethers[45,46] and slightly concaved dome is given for tazofelone.[13] There is also another nearly ideal but metastable solid solution δ present (metastable solid solutions have already been previously reported[47,48]). Similarly, there is no composition dependent variation of the enthalpy of melting. The liquidus and solidus of δ form a convex dome, which indicates on a slightly lower stability of the racemic composition phase. The observed convex behaviour is not typical for solid solutions showing miscibility around the racemic composition as mostly concave behaviour is reported.[13,14,16,17,45,46,49–51]

The very similar PXRD patterns observed for *enant*–F and *rac*–D (Figure 3) as well as melting data represented in the phase diagram might suggest that it is a single continuous solid solution in part of the composition range being metastable. However, results of the structural and SSNMR study of *enant*–F and *rac*–D presented later indicate that these phases are not completely isostructural thus confirming the existence of two distinct solid solutions. Finally, the solid solution γ is also metastable and like solid solution δ supposedly due to metastability can be accessed to only in a limited composition range. Forms *rac*–B and *enant*–E are depicted as metastable polymorphs, however, due to experimental limitations obtaining the forms, no strong statements could be made whether forms are strictly enantioselective, or is there any miscibility of the enantiomers possible.

The large amount of solid solutions found for pimobendan enantiomers is surprising and to the best knowledge of the authors no other compound is reported to show such a diversity of structures able to form single scalemic phases. Moreover, the list of solid solutions formed by pimobendan enantiomers does not end with non-solvated phases. *rac*–C ($\gamma_{X=50}$) could only

be obtained by desolvating the methanol hemisolvate *rac*–MS2 upon heating (see Figure 4), and because the transition from *rac*–MS2 to *rac*–C is direct (see the DSC curves in Figure 6 and data on transformation kinetics given in the Supporting Information), it follows that form MS2 itself must be a solid solution as well. Although an isopleth section of the ternary melt phase diagram could also be constructed, it meets additional experimental difficulties (DSC analysis must be carried out in hermetically sealed pans to avoid desolvation prior the melting. Furthermore, the interpretation of the data could be complicated if the solvate melts incongruently.). The existence of solid solutions of pimobendan methanol hemisolvate MS2 is thus proven by PXRD, TG, and DSC analysis. Figure 6 clearly shows that PXRD patterns of different enantiomeric composition samples are very similar as expected for solid solutions.[6,10,14,16] Furthermore, TG curves show that for example racemic and 30 % composition samples both loose approximately 4.6 % of the initial mass corresponding to 0.5 methanol molecules per one pimobendan molecule therefore excluding the existence of an additional minor phase of the excess enantiomer in the 30 % sample, that may be missed or overlooked in the PXRD analysis. In addition, the DSC curves show similar thermal behaviour.

Further exploration of the pimobendan solid forms revealed that majority of the solvates are actually solid solutions. Previously reported structural and stability study[40] of pimobendan monohydrates showed that structurally distinct racemic and enantiopure monohydrates (namely, *rac*–H1 and *enant*–H5) exist. It would be expected that scalemic mixtures would show enantioselectivity of pimobendan enantiomers — equimolar amounts of opposite enantiomers forming *rac*–H1 and the remaining excess enantiomer forming *enant*–H5. However, crystallizing scalemic pimobendan mixtures from solvents containing water, solid solutions formed instead. In Figure 7 PXRD patterns of H1 and H5 are depicted. Although PXRD patterns of the enantiopure and racemic monohydrates are very similar (due to the already described similarities of the structures[40]), PXRD patterns of scalemic mixtures are not superposition of *rac*–H1 and *enant*–H5 patterns. In fact, PXRD patterns of 46, 41, and 32 %

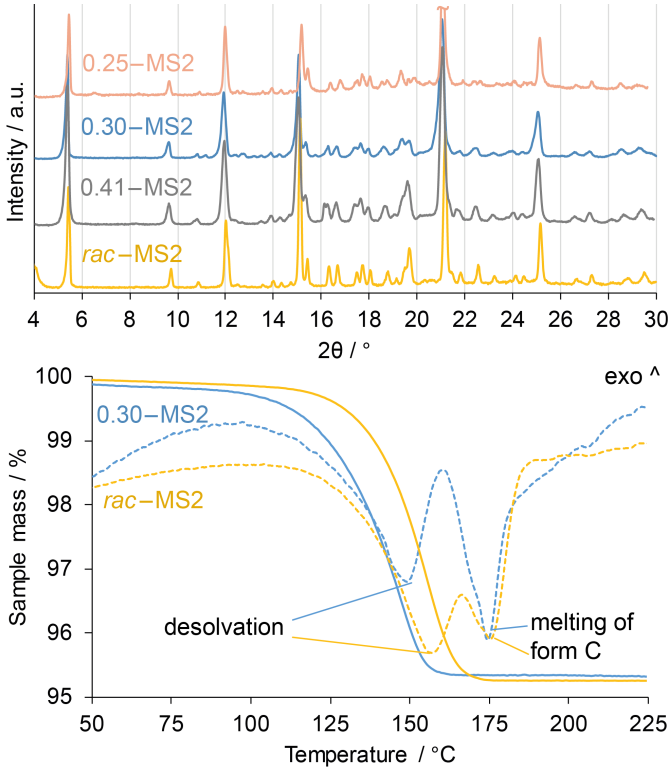

Figure 6: PXRD patterns, TG (solid lines) and DSC (dashed lines) curves of racemic and scalemic composition samples of pimobendan methanol hemisolvate MS2.

mixtures are more similar to that of *rac*–H1, whereas that of 10 % sample is more similar to *enant*–H5, with the corresponding peak positions and intensities slightly varying. Another proof that the scalemic composition samples are single phases (and not mixtures of *rac*–H1 and *enant*–H5) can be found in the recorded TG/DSC traces. Both monohydrates are reported to dehydrate at different temperatures, furthermore the dehydration products differ.[40] If there were different amounts of *rac*–H1 and *enant*–H5 present, the TG curve would contain two steps corresponding to the dehydration of each of the hydrates, however, TG curves of 46, 41, and 32 % composition samples are very smooth showing that the removal of water occurs in a single step (see Figure S8). Furthermore, DSC curves are similar to that of *rac*–H1 showing that similar dehydration product (amorphous phase) forms (see Figure S8). DSC curve of 10 % sample is similar to that reported for *enant*–H5[40] showing additional endothermic event corresponding to the melting of the poorly crystalline dehydration product E (see Figure S9). It can be concluded that *rac*–H1 and *enant*–H5 are in fact limiting cases

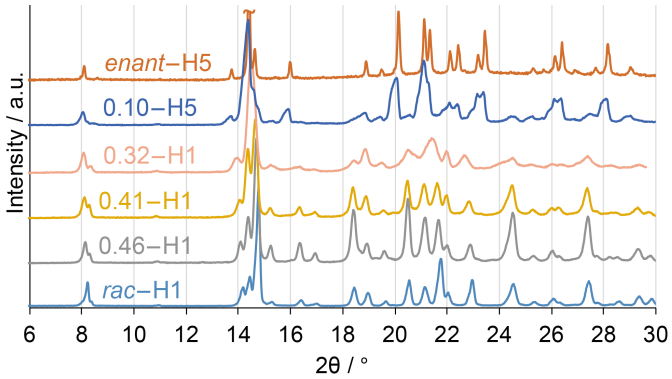

Figure 7: PXRD patterns of racemic, enantiopure, and scalemic composition samples of pimobendan monohydrates H1 and H5.

of two solid solutions apparently showing limited miscibility around the racemic and near the pure enantiomer composition regions, respectively.

Similarly, two pimobendan 1,4-dioxane monosolvates can be obtained — the already known *rac*–DS1 and *enant*–DS2 discovered in this study. Both solvates have similar PXRD patterns, however, careful examination of the patterns (Figure 8) of scalemic samples showed that those are not two extremes of one solid solution, but (similarly like in case of *rac*–H1 and *enant*–H5) there are two solid solutions — one around the racemic and the other near the pure enantiomer composition region. PXRD patterns show that *rac*–DS1, 0.41–DS1, and

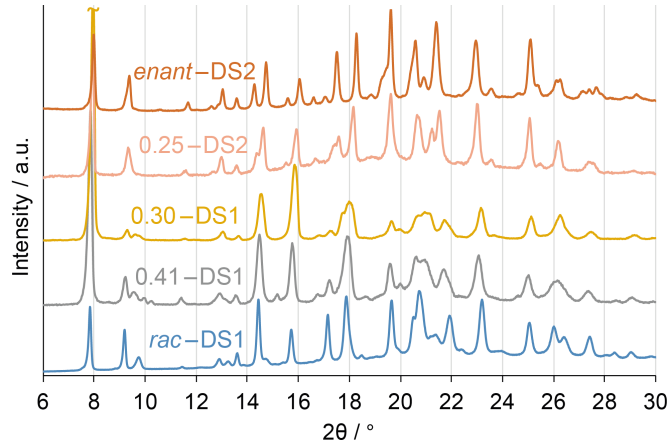

Figure 8: PXRD patterns of racemic, enantiopure, and scalemic composition samples of pimobendan 1,4-dioxane monosolvates DS1 and DS2.

0.30–DS1 are similar, furthermore peak broadening resulting from the increase of the disor-

der is observed. On contrary, 25 % sample resembles more that of *enant*–DS2. No smooth and continuous transition of the peak properties is present across the concentration range, but rather discontinuity can be observed between 25 and 30 % enantiomeric composition samples. Also the TG/DSC analysis show considerably different behaviour of 25 and 30 % phases (see Figure S10).

Considering the diversity of pimobendan crystal forms existing as solid solutions already discussed, it is not surprising that a few more of the remaining racemic solvates were found to be solid solutions showing at least some miscibility of the enantiomers around the racemic composition. For example, a single phase — solvate $G_{toluene}$ was obtained also for the 30 % composition sample as concluded from the PXRD data (see Figure S11) and TG analysis results (showing around 19 % weight loss similarly as for the *rac*–$G_{toluene}$). It is therefore likely that also other isostructural solvates G (containing another solvent) having scalemic compositions exist. Pimobendan hemihydrate H3 was found to exist as solid solution showing very similar PXRD patterns (see Figure S12) and around 2.5 % weight loss on heating corresponding to the hemihydrate. Furthermore, also pimobendan methanol monosolvate MS1 most likely represents another solid solution (Figure S13).

The large amount of solid solutions identified for both non-solvated and solvated pimobendan phases rises a question what are the underlying reasons responsible for the formation of those commonly extremely rare type of phases[3] in such a large diversity for a single compound. Structural study was performed to better explore the observed phenomenon.

Structural study of pimobendan solid forms

Previous studies have shown that there must be very specific structural features present for solid solutions to exist[6,7] which is the reason they occur so extremely rarely.[3] Surprisingly, in case of pimobendan almost all of the crystal forms found are convincingly proven to exist in a form of solid solutions (with the remaining crystalline phases being rather questionable not strongly proven to be completely enantioselective). Furthermore, solid solutions form

regardless of whether non-solvated or solvated phases are considered. It follows that the driving force of solid solution formation in this case could be tracked down to the molecular level.

Structural study of pimobendan crystal forms was performed to explore the structural aspects governing the solid solution formation. For racemic pimobendan single crystals, however, were obtained only in case of *rac*–A ($\alpha_{X=50}$) since it is the only racemic non-solvated form obtainable from a solution. Unfortunately, no single crystals were obtained for any of the solvates except for the racemic monohydrate *rac*–H1 already reported.[40] SCXRD structure of a monohydrate of enantiopure pimobendan (*enant*–H5) is also reported,[40] but no single crystals of any other enantiopure forms were obtained. Crystal structure determination from powder X-ray diffraction data of several phases was considered (the structure of *rac*–B from the PXRD data has already been reported[42]). The structure solution was successful and reliable only in the case of the enantiopure polymorph *enant*–F ($\zeta_{X=0}$). Furthermore, SSNMR spectroscopy served as a crucial technique to facilitate the structure determination. Selected crystallographic data of *rac*–A and *enant*–F are presented in Table 2.

Structure of *rac*–A

The asymmetric unit of *rac*–A (or $\alpha_{X=50}$) is a superimposition of both enantiomers R and S. Their occupancies are 0.74 and 0.26, respectively (see Figure 9). Each of the enantiomers occupies different conformation, e.g., RI and SII. Furthermore, concerning the apparent centrosymmetry of the structure there are also SI and RII conformers present (with the opposite occupancies giving overall racemic composition of the crystal). Thus, in the crystal structure of *rac*–A for every each pair of crystallographic molecular positions that are related by symmetry elements changing the handedness (centres of inversion and glide planes in this case) there is in fact a probability (approximately 3:1), whether a pair of pimobendan molecules is genuinely symmetric (RI–SI or RII–SII) or is it *quasi*–symmetric (RI–RII or

Table 2: Selected crystallographic data of pimobendan crystal structures *rac*–A and *enant*–F.

	rac–A *ss* $\alpha_{X=50}$	*enant*–F *ss* $\zeta_{X=0}$
Empirical formula	$C_{19}H_{18}N_4O_2$	$C_{19}H_{18}N_4O_2$
Formula weight / g mol^{-1}	334.37	334.37
T / K	293	293
Sample type	Single crystal	Powder
Crystal system	Monoclinic	Trigonal
Space group	$C2/c$	$P3_121$ ($P3_221$)
a / Å	16.9418(5)	9.3798(6)
b / Å	9.1256(3)	9.3798(6)
c / Å	22.9751(8)	33.194(3)
α / °	90	90
β / °	107.3133(16)	90
γ / °	90	120
V / Å^3	3391.11(19)	2529.2(5)
ρ_{calc} / g cm^{-3}	1.310	1.317
Z, Z'	8, 1	6, 1
Reflns. collected	3276	–
Reflns. with $I > 2\sigma(I)$	2132	–
R_1 ($I > 2\sigma(I)$)	0.0643	–
S	1.045	–
R_{wp} (R_p)	–	0.0740 (0.0494)

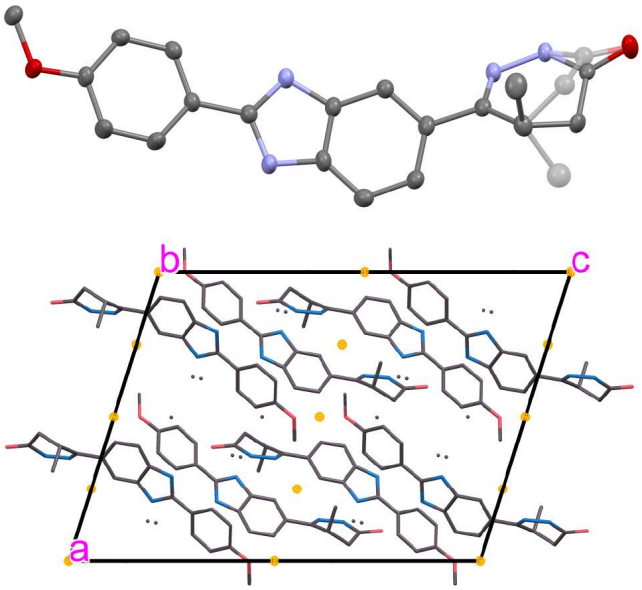

Figure 9: Asymmetric unit (showing the superimposition of both enantiomers with occupancy factors 0.74 and 0.26) and packing representation (centres of inversion depicted in yellow) of pimobendan *rac*–A . Hydrogen atoms omitted for the sake of clarity.

SI–SII). Note that according to the determined structure there are never RI–SII or RII–SI pairs present if the locus of symmetry for the pair of two crystallographic positions is an inversion centre or a glide plane. Therefore, as the occupancy of both enantiomers is not 1:1, there is inevitably some degree of enantioselectivity present. The structure tend to be an ordinary racemic compound. Furthermore, it can be noted that same chirality conformers I and II found in the crystal structure are approximate mirror images to each other ensuring *quasi*–centrosymmetric (or *quasi*–glide-symmetric) relationship. Structural origin of solid solution existence for *rac*–A (as proved by the melt phase diagram represented in the Figure 5) is therefore evident. It is comprehensible that in scalemic crystals more *quasi*–symmetric pairs of the enantiomer in majority may form in that way preserving the apparent centrosymmetry and general packing of the structure. Because of the observed structural aspects present and, thus, partial enantioselectivity in the solid state, the solid solution α is Type II solid solution.

Structure of *enant*–F

(*R*)–pimobendan was found to crystallize in $P3_121$ space group. As it is one of the 11 enantiomorphic pairs of chiral space groups, the structure of the opposite enantiomer belongs to the $P3_221$ space group. The ^{13}C SSNMR spectrum was simulated to compare that with the experimentally obtained one by thus assessing if the structure solved from the PXRD data is reasonable (see Figure 10). A good fit between the experimental and theoretical values is obtained. The largest differences from the fitted straight line are observed for both methyl groups which could be explained by relative freedom of those substituents in the crystal structure. Furthermore, the SSNMR spectrum was also exploited to define the structural aspects of pimobendan solid solution ζ. The spectrum (Figure 11) of *enant*–F ($\zeta_{X=0}$) convincingly shows that there is only one pimobendan molecule in the asymmetric unit ($Z' = 1$). As $Z' = 1$ it follows that no partial enantioselectivity is possible and it

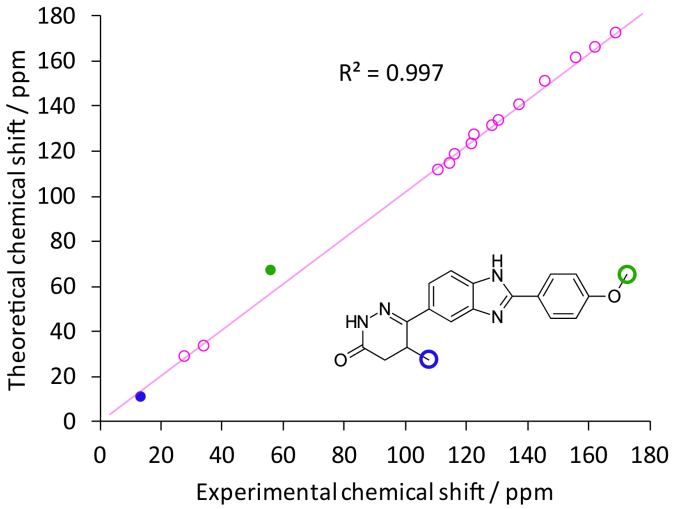

Figure 10: Correlation between the theoretical and experimentally determined chemical shifts in ^{13}C SSNMR spectra of *enant*–F.

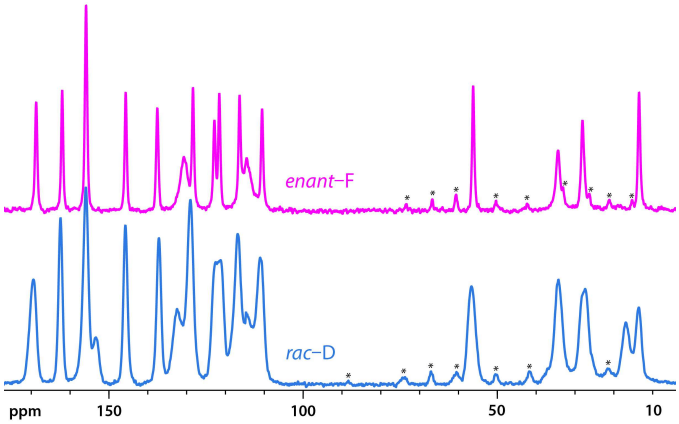

Figure 11: ^{13}C SSNMR spectra of *enant*–F and *rac*–D (spinning side-bands depicted with an asterisk).

indicates that solid solution ζ is of a Type I. Moving towards racemic composition statistically there will be a probability of finding R or S enantiomer in any molecular site equal to mole fraction of R or S enantiomer in the crystal, respectively. Inevitably it leads that probability of finding R or S molecule in any molecular site for such structure is exactly 50 % for racemic composition. SSNMR spectra of *enant*–F and *rac*–D were compared to elucidate whether those phases could be isostructural corresponding to limiting cases of only one solid solution, or are they rather limiting cases of two distinct solid solutions. Peak count of *rac*–D spectrum indicates that also there is only one pimobendan molecule in the

asymmetric unit ($Z' = 1$). The peaks are broader indicating that *rac*–D is considerably disordered. Although the PXRD patterns of both forms are very similar (Figure 3) and the melting data of corresponding scalemic phases could be interpreted as belonging to a single continuous solid solution (Figure 5), further analysis of the SSNMR data confirms the presence of two distinct solid solutions. The two additional peaks (at around 17 and 153 ppm) in the spectrum of *rac*–D indicate on the static disorder. However, the split (same atom) peak area ratio is not 1:1, indicating that one of the conformer is more abundant in the crystal structure of *rac*–D. If *rac*–D was the limiting case of the solid solution ζ, then at racemic composition as mentioned before probability of finding one enantiomer in a crystallographic molecular site would be exactly 50 % consequently giving equal areas for the split atom peaks. As it is not so, by definition solid solution δ cannot be Type I solid solution, but on contrary there is some enantioselectivity present leading to Type II for δ.

Similarities and differences of *rac*–A and *enant*–F structures

The stability of a crystal structure is ensured by favourable intermolecular interactions. Pimobendan molecule has several electron-donor/acceptor sites as well as aromatic rings that can be exploited to form such favourable interactions in a form of hydrogen bonds or $\pi \cdots \pi$ sackings. In the structure of *rac*–A and *enant*–F hydrogen bonds are present (Figure 12). In both cases none of the chiral carbon substituents are directly involved in hydrogen bond network which is undoubtedly the main stabilizing force determining the stability of the crystal structures. Existence of solid solutions α and ζ can be therefore explained by the fact that apparently due to conformational flexibility the hydrogen bond network can be preserved regardless of which enantiomer is exploited similarly like in case of, e.g., two solid solutions reported for phenylpiracetam,[6] a chiral pyrrolidine derivative,[52] and drugs tazofelone[13] and atenolol.[15]

Hydrogen networks in both structures in fact are identical (see the representation in Figure 13). There are $R_2^2(16)$ rings and $C_1^1(11)$ chains present. The differences between the

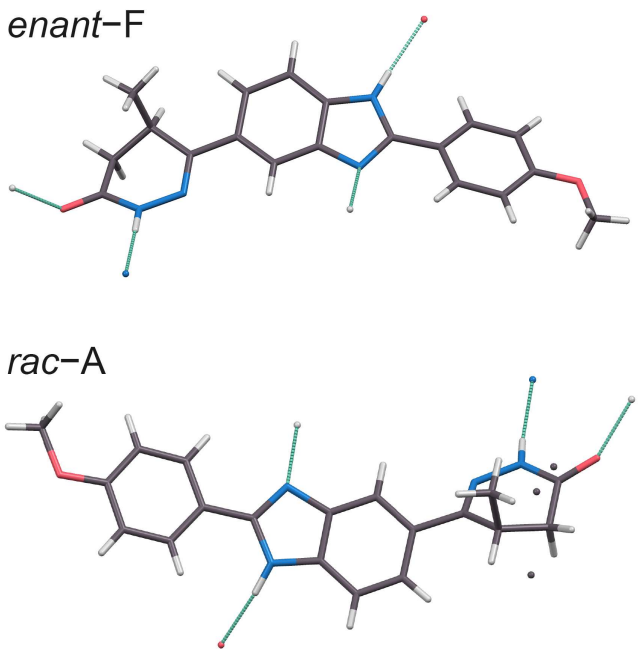

Figure 12: Asymmetric units of pimobendan *rac*–A and *enant*–F showing hydrogen bonds.

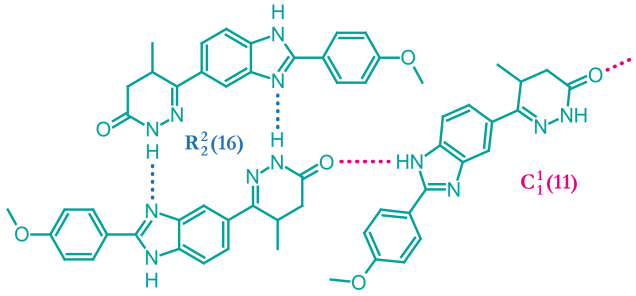

Figure 13: Representation of hydrogen bond network in the structures of *rac*–A and *enant*–F.

structures are found in molecule conformations and packing of the molecules. In the structure of *rac*–A the molecules forming $R_2^2(16)$ rings are (*quasi*–)centrosymmetric, while in that of *enant*–F they are not even close to centrosymmetry. In the structure of *rac*–A the infinite $C_1^1(11)$ chains stacked parallel are forming layers which are interconnected via before mentioned $R_2^2(16)$ hydrogen bonds. In *enant*–F the $C_1^1(11)$ chains form rods which have 3-fold screw axis symmetry. The rods are interconnected via $R_2^2(16)$ hydrogen bonds (see Figure 14).

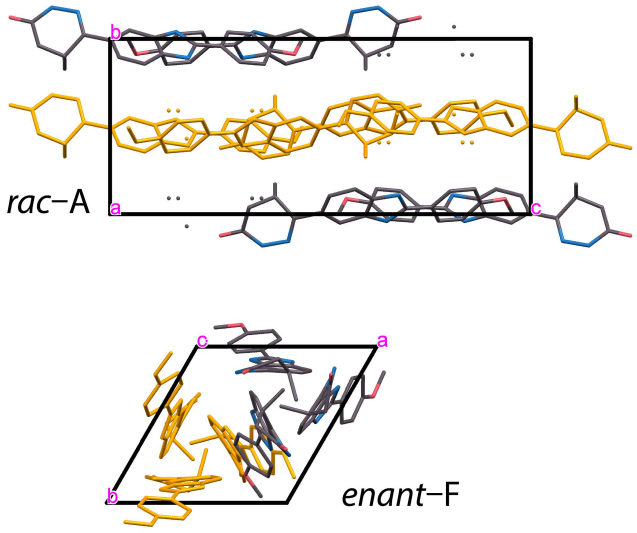

Figure 14: Packing representation of *rac*–A and *enant*–F along the crystallographic a, and c–axis, respectively. Layers and rods formed via $C_1^1(11)$ hydrogen bonds shown in orange.

Conclusions

In this and previous studies of the authors the pharmaceutically active ingredient pimobendan was found to form 5 racemic and 2 enantiopure polymorphs as well as 8 racemic and 2 enantiopure solvates. Surprisingly, 4 of 6 polymorphic forms were proven to exist as solid solutions consequently showing limited or no enantioselectivity in the solid state. Furthermore, also at least 7 out of 10 solvates were found to be solid solutions. None of the 11 solid solutions exist in the full composition range. Therefore for a distinct set of racemic and a

distinct set of enantiopure structures there is an ability to host amounts of (excess or the opposite) enantiomer preserving the crystal structure. The considerable number of different structures (non-solvated and solvated) that may be obtained as single phases of scalemic compositions means that the driving force of solid solution formation could be tracked down to molecular structure level.

As the chiral centre is fixed in a pyridazinone cycle with the remaining two substituents being a hydrogen atom and a methyl group, it is assumed that the lack of the enantioselectivity is as follows: the changes introduced by placing one or another enantiomer in a crystallographic molecular position are not crucial, because in terms of intermolecular interactions: 1) no steric effect hindrance is expected because of comparable sizes of the non-ring chiral centre substituents; 2) only dispersion energy term is affected by the change, which obviously has a minor importance determining the lattice energy as efficient hydrogen bond network can be expected. The mentioned reasons are in agreement with the two determined crystal structures. Furthermore, the most crucial aspect of solid solution formation is molecular flexibility which allows to maintain the hydrogen bond network regardless of the configuration of the chiral centre of pimobendan molecule. The study also showed that solid solutions α and δ is Type II solid solutions which means there is some enantioselectivity in the solid state while solid solution ζ is Type I solid solution — without any enantioselectivity.

Finally, it is intriguing that none of the solid solutions exist in the whole enantiomeric composition range. Although crystallographic molecular positions in pimobendan polymorph and solvate crystal structures seem to be fairly indifferent regarding both enantiomers, different structures form at two extreme cases — racemic and enantiopure compositions. It shows that apparently it is energetically more favourable to pack racemic (or close-to-racemic) composition systems differently than those of enantiopure (or close-to-enantiopure) composition.

Supporting Information Available

The crystal structure data (CIF), transition scheme between pimobendan forms, preparation of pimobendan forms, thermal analysis of pimobendan forms, DSC and PXRD data used to establish the phase diagram of pimobendan enantiomers, evidence of solvated pimobendan solid solutions, experimental and calculated PXRD patterns of pimobendan polymorph *enant*–F. This material is available free of charge via the Internet at `http://pubs.acs.org/`.

References

(1) Rouhi, A. M. Chiral Business. *Chemical & Engineering News Archive* **2003**, *81*, 45–61.

(2) Lorenz, H.; Seidel-Morgenstern, A. Processes To Separate Enantiomers. *Angewandte Chemie International Edition* **2014**, *53*, 1218–1250.

(3) Jacques, J.; Collet, A.; Wilen, S. *Enantiomers, racemates, and resolutions*; Wiley, 1981.

(4) Kaemmerer, H.; Lorenz, H.; Black, S. N.; Seidel-Morgenstern, A. Study of System Thermodynamics and the Feasibility of Chiral Resolution of the Polymorphic System of Malic Acid Enantiomers and Its Partial Solid Solutions. *Cryst. Growth Des.* **2009**, *9*, 1851–1862.

(5) Kotelnikova, E. N.; Isakov, A. I.; Lorenz, H. Non-equimolar discrete compounds in binary chiral systems of organic substances. *CrystEngComm* **2017**, *19*, 1851–1869.

(6) Rekis, T.; Bērziņš, A.; Orola, L.; Holczbauer, T.; Actiņš, A.; Seidel-Morgenstern, A.; Lorenz, H. Single enantiomer's urge to crystallize in centrosymmetric space groups: solid solutions of phenylpiracetam. *Cryst. Growth Des.* **2017**, *17*, 1411–1418.

(7) Brandel, C.; Petit, S.; Cartigny, Y.; Coquerel, G. Structural Aspects of Solid Solutions of Enantiomers. *Current Pharmaceutical Design* **2016**, *22*, 4929–4941.

(8) Chion, B.; Lajzerowicz, J.; Bordeaux, D.; Collet, A.; Jacques, J. Structural aspects of solid solutions of enantiomers: the 3-hydroxymethyl- and 3-carboxy-2,2,5,5-tetramethylpyrrolidinyl 1-oxyl systems as examples. *The Journal of Physical Chemistry* **1978**, *82*, 2682–2688.

(9) Bordeaux, D.; Lajzérowicz, J. Structure cristalline du tétraméthyl-2,2,6,6 (hydroxyimino)-4 pipéridine oxyl-1. *Acta Crystallographica Section B* **1977**, *33*, 1837–1840.

(10) Taratin, N. V.; Lorenz, H.; Kotelnikova, E. N.; Glikin, A. E.; Galland, A.; Dupray, V.; Coquerel, G.; Seidel-Morgenstern, A. Mixed Crystals in Chiral Organic Systems: A Case Study on (R)- and (S)-Ethanolammonium 3-Chloromandelate. *Cryst. Growth Des.* **2012**, *12*, 5882–5888.

(11) Wermester, N.; Aubin, E.; Pauchet, M.; Coste, S.; Coquerel, G. Preferential crystallization in an unusual case of conglomerate with partial solid solutions. *Tetrahedron: Asymmetry* **2007**, *18*, 821 – 831.

(12) Rekis, T.; D'Agostino, S.; Braga, D.; Grepioni, F. Designing solid solutions of enantiomers: lack of enantioselectivity of chiral naphthalimide derivatives in the solid state. *Crystal Growth & Design* **0**, *0*, null.

(13) Huang, J.; Chen, S.; Guzei, I. A.; ; Yu, L. Discovery of a Solid Solution of Enantiomers in a Racemate-Forming System by Seeding. *Journal of the American Chemical Society* **2006**, *128*, 11985–11992.

(14) de Diego, H. L.; Bond, A. D.; Dancer, R. J. Formation of solid solutions between racemic and enantiomeric citalopram oxalate. *Chirality* **2011**, *23*, 408–416.

(15) de Castro, R. A. E.; Canotilho, J.; Barbosa, R. M.; Silva, M. R.; Beja, A. M.; Paixão, J. A.; Redinha, J. S. Conformational Isomorphism of Organic Crystals: Racemic and Homochiral Atenolol. *Cryst. Growth Des.* **2007**, *7*, 496–500.

(16) Vogt, F. G.; Copley, R. C. B.; Mueller, R. L.; Spoors, G. P.; Cacchio, T. N.; Carlton, R. A.; Katrincic, L. M.; Kennady, J. M.; Parsons, S.; Chetina, O. V. Isomorphism, Disorder, and Hydration in the Crystal Structures of Racemic and Single-Enantiomer Carvedilol Phosphate. *Cryst. Growth Des.* **2010**, *10*, 2713–2733.

(17) Bredikhin, A. A.; Bredikhina, Z. A.; Zakharychev, D. V.; Gubaidullin, A. T.; Fayzullin, R. R. Chiral drug timolol maleate as a continuous solid solution: Thermochemical and single crystal X-ray evidence. *CrystEngComm* **2012**, *14*, 648–655.

(18) Gordon, S. G.; Miller, M. W.; Saunders, A. B. Pimobendan in Heart Failure Therapy - A Silver Bullet? *Journal of the American Animal Hospital Association* **2006**, *42*, 90–93.

(19) Chu, K. M.; Shieh, S. M.; Hu, O. Y. Pharmacokinetics and pharmacodynamics of enantiomers of pimobendan in patients with dilated cardiomyopathy and congestive heart failure after single and repeated oral dosing. *Clinical pharmacology and therapeutics* **1995**, *57*, 610–621.

(20) Austel, V.; Noll, K.; Eberlein, W.; Heider, J.; Van Dr Meel, J.; Diederen, W.; Haarmann, W. Neue (-)-benzimidazole, deren herstellung und diese verbindungen enthaltende arzneimittel. 1989; `https://encrypted.google.com/patents/DE3728244A1?cl=it`, DE Patent App. DE19,873,728,244.

(21) Sheldrick, G. M. A short history of SHELX. *Acta Crystallographica Section A: Foundations of Crystallography* **2007**, *64*, 112–122.

(22) Altomare, A.; Cuocci, C.; Giacovazzo, C.; Moliterni, A.; Rizzi, R.; Corriero, N.; Falcicchio, A. EXPO2013: a kit of tools for phasing crystal structures from powder data. *J. Appl. Crystallogr.* **2013**, *46*, 1231–1235.

(23) Altomare, A.; Campi, G.; Cuocci, C.; Eriksson, L.; Giacovazzo, C.; Moliterni, A.;

Rizzi, R.; Werner, P. E. Advances in powder diffraction pattern indexing: N-TREOR09. *J. Appl. Crystallogr.* **2009**, *42*, 768–775.

(24) Boultif, A.; Louer, D. Powder pattern indexing with the dichotomy method. *J. Appl. Crystallogr.* **2004**, *37*, 724–731.

(25) Le Bail, A.; Duroy, H.; Fourquet, J. L. Ab-initio structure determination of LiSbWO6 by X-ray powder diffraction. *Mater. Res. Bull.* **1988**, *23*, 447–452.

(26) Dollase, W. A. Correction of intensities for preferred orientation in powder diffractometry: application of the March model. *J. Appl. Crystallogr.* **1986**, *19*, 267–272.

(27) March, A. Z. Mathematische Theorie der Regelung nach der Korngestalt bei affiner Deformation. *Kristallogr.* **1932**, *81*, 285–297.

(28) Giannozzi, P. et al. QUANTUM ESPRESSO: a modular and open-source software project for quantum simulations of materials. *Journal of Physics: Condensed Matter* **2009**, *21*, 395502.

(29) Grimme, S. Semiempirical GGA-type density functional constructed with a long-range dispersion correction. *Journal of Computational Chemistry* **2006**, *27*, 1787–1799.

(30) Lund, A. M.; Orendt, A. M.; Pagola, G. I.; Ferraro, M. B.; Facelli, J. C. Optimization of Crystal Structures of Archetypical Pharmaceutical Compounds: A Plane-Wave DFT-D Study Using Quantum Espresso. *Crystal Growth & Design* **2013**, *13*, 2181–2189.

(31) Morcombe, C. R.; Zilm, K. W. Chemical shift referencing in {MAS} solid state {NMR}. *Journal of Magnetic Resonance* **2003**, *162*, 479 – 486.

(32) Pickard, C. J.; Mauri, F. All-electron magnetic response with pseudopotentials: NMR chemical shifts. *Phys. Rev. B* **2001**, *63*, 245101.

(33) Clark, S.; Segall, M.; Pickard, C.; Hasnip, P.; Probert, M.; Refson, K.; Payne, M. First principles methods using CASTEP. *Zeitschrift für Kristallographie* **2005**, *220*, 567–570.

(34) Yates, J.; Pickard, C.; Mauri, F. Calculation of NMR chemical shifts for extended systems using ultrasoft pseudopotentials. *Physical Review. B, Condensed matter and materials physics* **2007**, *76*.

(35) Harris, R. K.; Hodgkinson, P.; Pickard, C. J.; Yates, J. R.; Zorin, V. Chemical shift computations on a crystallographic basis: some reflections and comments. *Magnetic Resonance in Chemistry* **2007**, *45*, S174–S186.

(36) Perdew, J. P.; Burke, K.; Ernzerhof, M. Generalized Gradient Approximation Made Simple. *Phys. Rev. Lett.* **1996**, *77*, 3865–3868.

(37) Tkatchenko, A.; Scheffler, M. Accurate Molecular Van Der Waals Interactions from Ground-State Electron Density and Free-Atom Reference Data. *Phys. Rev. Lett.* **2009**, *102*, 073005.

(38) Bērziņš, A.; Hodgkinson, P. Solid-state {NMR} and computational investigation of solvent molecule arrangement and dynamics in isostructural solvates of droperidol. *Solid State Nuclear Magnetic Resonance* **2015**, *65*, 12 – 20.

(39) Boeren, M. M. M.; Paridaans, R. J.; Petkune, S.; Lusis, V.; Muceniece, D. Crystalline pimobendan, process for the preparation thereof, pharmaceutical composition and use. 2014.

(40) Rekis, T.; Bērziņš, A.; Džabijeva, D.; Nakurte, I.; Orola, L.; Actiņš, A. Structure and stability of racemic and enantiopure pimobendan monohydrates: on the phenomenon of unusually high stability. *Cryst. Growth Des.* **2017**, *17*, 1814–1823.

(41) Rekis, T.; Oša, G.; Bērziņš, A.; Actiņš, A. Process for preparation of crystalline form A of pimobendan. 2013.

(42) Zvirgzdins, A.; Delina, M.; Mishnev, A.; Actins, A. Pimobendan B from powder diffraction data. *Acta Crystallographica Section E* **2013**, *69*, o1677.

(43) Hilfiker, R. *Polymorphism: In the Pharmaceutical Industry*; 2006; pp 1–414.

(44) Coquerel, G. Review on the heterogeneous equilibria between condensed phases in binary systems of enantiomers. *Enantiomer* **2000**, *5*, 481 – 498.

(45) Bredikhin, A. A.; Bredikhina, Z. A.; Zakharychev, D. V. Crystallization of chiral compounds: thermodynamical, structural and practical aspects. *Mendeleev Communications* **2012**, *22*, 171 – 180.

(46) Fayzullin, R. R.; Zakharychev, D. V.; Gubaidullin, A. T.; Antonovich, O. A.; Krivolapov, D. B.; Bredikhina, Z. A.; Bredikhin, A. A. Intricate Phase Behavior and Crystal Structure Features of Chiral para-Methoxyphenyl Glycerol Ether Forming Continuous and Partial Solid Solutions. *Cryst. Growth Des.* **2017**, *17*, 271–283.

(47) Brandel, C.; Amharar, Y.; Rollinger, J. M.; Griesser, U. J.; Cartigny, Y.; Petit, S.; Coquerel, G. Impact of Molecular Flexibility on Double Polymorphism, Solid Solutions and Chiral Discrimination during Crystallization of Diprophylline Enantiomers. *Molecular Pharmaceutics* **2013**, *10*, 3850–3861.

(48) Bredikhin, A. A.; Bredikhina, Z. A.; Antonovich, O. A.; Zakharychev, D. V.; Krivolapov, D. B. Crystallization features and spontaneous resolution of 3-(2,6-dimethoxyphenoxy)propane-1,2-diol: The case of stable conglomerate and metastable solid solution. *Journal of Molecular Structure* **2017**, *1144*, 443 – 450.

(49) Li, Y.; Zhao, Y.; Zhang, Y. Solid Tryptophan as a Pseudoracemate: Physicochemical and Crystallographic Characterization. *Chirality* **2015**, *27*, 88–94.

(50) Gallis, H.; Bougrioua, F.; Oonk, H.; van Ekeren, P.; van Miltenburg, J. Mixtures of d- and l-carvone: I. Differential scanning calorimetry and solid-liquid phase diagram. *Thermochimica Acta* **1996**, *274*, 231 – 242.

(51) Oonk, H.; Tjoa, K.; Brants, F.; Kroon, J. The carvoxime system. *Thermochimica Acta* **1977**, *19*, 161 – 171.

(52) Lajzerowicz, J.; Chion, B.; Lajzerowicz, J. Two dimensional order in a solid solution of molecules of opposite chirality. *The Journal of Chemical Physics* **1981**, *74*, 3500–3509, cited By 5.

For Table of Contents Use Only

A maze of solid solutions of pimobendan enantiomers: an extraordinary case of polymorph and solvate diversity

Toms Rekis, Agris Bērziņš, Inese Sarceviča, Artis Kons, Mārtiņš Balodis, Liāna Orola, Heike Lorenz, and Andris Actiņš

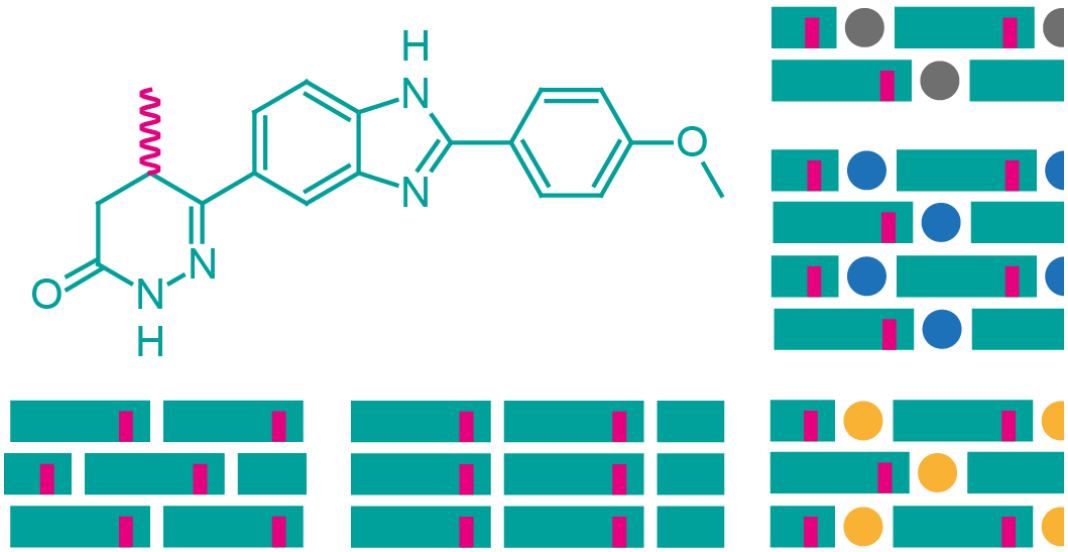

Several polymorphs and solvates are found for racemic and enantiopure pimobendan. Most of them are proven to exist as solid solutions of enantiomers. Structural study shows the origin of solid solution formation. The reasons of their formation in such a large diversity for a single compound are tracked down to molecular level.